International Journal on Interactive Design and Manufacturing (IJIDeM) (2024) 18:5501–5513
https://doi.org/10.1007/s12008-024-01796-0

ORIGINAL ARTICLE

Thermal evaluation of aluminum welding: a comparative study of friction stir welding (FSW), plasma-fsw, and tungsten inert gas (TIG)-FSW techniques

Deepak Kumar Yaduwanshi[1] · Chennu Rama Mohan Rao[2] · S. C. V. Ramana Murty Naidu[3] · Sanjay G. Sakharwade[4] · Sumit Sharma[5] · V. Khalkar[6] · S. Baskar[7] · Gopal Kaliyaperumal[8]

Received: 1 November 2023 / Accepted: 9 March 2024 / Published online: 21 April 2024

Abstract

This research work presents the comparative analysis of heat input during aluminum welding focusing on FSW, Plasma-FSW, and TIG–FSW. This study aims to investigate their thermal behavior and temperature distributions during aluminum welding. With a specific emphasis on their thermal histories, peak temperatures, and simulated weld zones, the study elucidates the impact of auxiliary heat sources on heat input and material flow. A comparison of the heat input, heat dissipation, and heat output of these three welding techniques is necessary for analyzing their weld characteristics. In this research work, ABAQUS software was utilized to develop a computational model and numerical simulation for analyses the thermal aspect of each welding technique. Welding parameters such as heat generation by tool, preheating by auxiliary heat source (electric arc at 45 amp) and welding speed (63 mm/min) are considered to understand heat distribution within the weld zone are evaluated and compared to justify the improvement and development of FSW technique of discrete artefacts. The influence of auxiliary heat source by Plasma arc and TIG arc show improvement in thermal behavior of welding such as peak temperature achieved percentages between 50 and 55% of melting temperature of base metal as compare to FSW (44.4%), indicating enhanced plasticization due to the additional heat provided by preheating sources. However, plasma-FSW achieved higher peak temperature due to stable, higher arc efficiency and high-energy nature of plasma arc preheating which create improved preheating zone with higher temperature. Therefore, the auxiliary source preheating proved crucial for adjusting the characteristics of the plasticized material and regulating the heat input before the FSW process. These results open up new avenues for research in hybrid FSW and encourage efficiency and creativity in welding technology for a variety of industrial applications. They also offer insightful information on how variations in heat input impact thermal behaviour and weld characteristics.

Keywords Comparative analysis · Thermal analysis · Aluminum welding · Friction stir welding (FSW) · Plasma-FSW · TIG–FSW · Hybrid friction stir welding

✉ S. Baskar
baskar133.se@velsuniv.ac.in

[1] Department of Mechanical Engineering, School of Engineering and Technology, IIMT University, Meerut, Uttar Pradesh 250001, India

[2] Department of Mechanical Engineering, Aditya College of Engineering, Surampalem, Andhra Pradesh 533437, India

[3] Department of Mechanical Engineering, Sri Venkateswara College of Engineering and Technology, Etcherla, Srikakulam, Andhra Pradesh 532410, India

[4] Department of Mechanical Engineering, Rungta College of Engineering and Technology, Bhilai, Chhattisgarh 490024, India

[5] Department of Mechanical Engineering, Poornima College of Engineering, Jaipur, Rajasthan 302022, India

[6] Department of Mechanical Engineering, Gharda Institute of Technology, Ratnagiri, Maharashtra 415708, India

[7] School of Engineering, Vels Institute of Science, Technology & Advanced Studies, Chennai, Tamil Nadu 600117, India

[8] Department of Mechanical Engineering, New Horizon College of Engineering, Bangalore, Karnataka 560103, India

1 Introduction

The search for efficient and effective welding procedures has been of utmost significance in the fields of modern industry and engineering. Traditional welding techniques have been crucial in producing structures and components, but technological improvements have sparked the investigation of alternative strategies to solve current constraints and improve weld quality [1]. The idea of hybrid FSW, which combines the fundamentals of traditional FSW with extra energy sources, both thermal and mechanical, is one such groundbreaking innovation [2]. It also emphasizes the design and practical implementation of hybrid manufacturing technique to real word problem. As a result of the combination of these techniques, welding operations are expected to change for the better thanks to improved weld characteristics, increased process efficiency, and wider application options [3–6].

A critical component of all welding procedures is controlled heat input. Controlled heat input is crucial in establishing the welded joint's mechanical characteristics, thermal behaviour, and joint quality. In friction stir welding (FSW), a specially designed FSW tool is rotated and translated to generate frictional heat. Also, during FSW, heat input is primarily determined by tool rotating speed, welding velocity, and perpendicular force between tool and workpiece which directly affect tool in the form of wear and failure of tool [5–9]. In a weld zone, higher rotational speeds and axial forces result in an increase in heat input, which has direct effect on the heat distribution, thermal gradients, and material flow. It is essential to control the heat input during FSW in order to achieve the desired weld properties and avoid defects like inadequate penetration and voids. By adapting a hybrid and integrated approach, the drawback allied with the FSW tool, such as wear, material compatibility, process optimization, and weld quality, can be addressed or improved. To overcome these imitation FSW is integrated with another welding process for better flexibility and control, resulting in enhanced tool life, expanded material compatibility, optimized process parameters, and improved weld quality. The variation in heat input among aluminum welding techniques examined in this research work—Friction Stir Welding (FSW), Plasma-FSW, and TIG–FSW can have important implications. The principle of FSW is based on the generation of frictional heat by rotating and translating specially designed tools. In FSW, a control the heat generated by friction and plastic deformation plays critical role in order to achieve the desired weld properties and prevent defects such as insufficient plastic deformation or material flow [11]. Therefore, this study is concentrated on two hybrid FSW technique Plasma-FSW and TIG–FSW. Plasma-FSW integrates the benefits of plasma arc welding with FSW. This technique uses a plasma arc to heat the workpiece before passing the FSW tool through it. However, Tungsten Inert Gas (TIG)–FSW integrate the additional heat input by TIG and an inert gas shield for protection during welding [12]. TIG and Pasma heat sources are controlled carefully so that the material ahead of the FSW process is also preheated, thus reducing the heat input by the FSW tool to the plasticized material as shown in Fig. 1. It is essential to understand how heat input affects the welding in order to optimize the parameters and achieve high-quality welding. The impartial of this research work is to provide insights into how different welding techniques influence thermal behavior and resulting weld characteristics in aluminum by comparing the heat input variations among FSW, Plasma-FSW, and TIG–FSW. In order to ensure efficient and effective aluminum welding, the findings will help determine the optimal heat input range for each method.

The many complex problems with traditional welding techniques are what spurred the adoption of hybrid FSW. Despite FSW With its solid-state joining mechanism, FSW has revolutionized welding, but it is not immune to limitations when working with specific materials and applications [5, 12–30]. HFSW seeks to overcome these obstacles and take advantage of synergistic effects that result in higher weld quality and process adaptability. This is accomplished through the creative integration of thermal and mechanical energy. Researchers have cleared the road for improvements that address plasticity, material flow, and joint characteristics by enhancing FSW with energy sources like electrical currents, laser heat, induction heating, ultrasonic vibrations, and even arc heating. In previous research comparative thermal analysis was not conducted so, control over heat input is essential, especially in Hybrid-FSW, where factors like comparative study on auxiliary heat sources and intensity of heat source directly affect material flow and heat distribution. In order to further the continued development of welding technology, this study explores the many methods of thermally and mechanically aided HFSW, their theoretical foundations, experimental implementations, and their potential influence across industries [5–14].

This work is devoted to analytical design and evaluating the complex interactions between heat input changes and welding processes thermally in the context of aluminium welding. The goal is to understand the complicated interaction between heat input, thermal behaviour, and the final weld properties by comparing the heat input changes between three different welding techniques: friction stir welding (FSW), Plasma-FSW, and TIG–FSW. Based on the incorporation of additional heat sources like plasma arcs or TIG heating, each approach presents a distinct heat input modulation. This investigation aims to identify the ideal heat input range for each technique in addition to unravelling the complex intricacies of heat input's influence. This thorough examination has provided a clearer comprehension of how various welding techniques can impact thermal dynamics and aluminium weld characteristics can be revealed, opening the door for

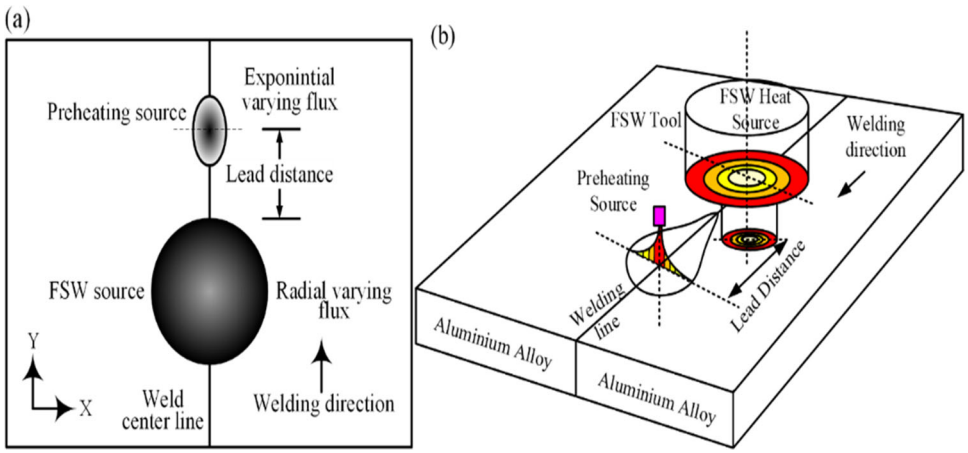

Fig. 1 Schematic illustration of heat source of FSW and preheating in hybrid FSW **a** Top view **b** Isometric view

designing a hybrid manufacturing technique and parameter optimisation to produce flawless welds and promote successful aluminium welding techniques.

2 Theoretical background

FSW is typically performed by inserting a spinning tool into the joint between two firmly fastened sheets, once the tool's shoulder has made contact with the surface of the material to be welded, press the tool down the weld line. Materials are joined by heat from plastic deformation and frictional heat when a normal force is applied [7]. Frictional heat from the tool shoulder is the main source of heat, and deformation heat from the tool pin is the secondary source [2]. Even though it produces the majority of the heat during the process, the shoulder also acts as the tool's primary barrier to material ejection and as the driving force behind material flow around it. The source of heat and the main cause of material deformation is the pin. In Fig. 2, various thermally and mechanically impacted zones are schematically depicted. In hybrid friction stir welding, the workpiece is heated up further just before to the weld zone, which lowers the mechanical energy demand on the tool. To pre-heat the workpiece, a variety of hybrid technologies have been developed.

These technologies could decrease tool forces, improve the plastic state, and have an indirect impact on tool life. Overall, in hybrid FSW systems, temperature regulation of the welded zone is essential.

At the point of contact between the tool and the workpiece, heat generation due to friction (Q_f) and heat generation due to plastic deformation (Q_p) combine to produce heat. Given this, the equation for the total heat produced by friction and plastic deformation is [18]

$$dQ_{FSW} = dQ_f + dQ_p \tag{1}$$

The material flow and heat generation at the interface are determined by contact characteristics, which are classified as sliding, sticking, or partial sliding/sticking circumstances [2]. The contact state under the shoulder can be ascertained by sliding friction or sticking friction, depending on the interfacial shear strength at the appropriate temperature and strain rate. The velocity of the tool surface and the velocity of the contact workpiece surface are connected by the readily specified contact state variable. It is believed that the contact state variable (δ) evolves linearly with increasing distance from the pin's centre. With the help of these assumptions and the geometric properties of the deformation zone, the contact state variable during friction heat generation condition can be expressed as [18]:

$$\delta = \frac{V_{matrix}}{V_{tool}} \tag{2}$$

where V_{tool} is the circumferential velocity of the FSW tool, and V_{matrix} is the circumferential velocity of the workpiece material. At the pin/material interface, a 100% sticking condition the same as tool velocity is assumed. At the outer border of the deformation, the material's velocity is equal to zero. Therefore, the contact shear stress will be [19]:

$$\tau_{contact} = \tau_y = \frac{\sigma_y}{\sqrt{3}} \tag{3}$$

The matrix segment volume shears slightly to a stationary elastic deformation where the shear stress equals the "dynamic" contact shear stress if the contact shear stress is less than the matrix shear yield stress. The term "sliding condition" describes this situation. The critical friction stress required for a sliding condition is described as follows by Coulomb's friction law [19]:

$$\tau_{contact} = \mu p \tag{4}$$

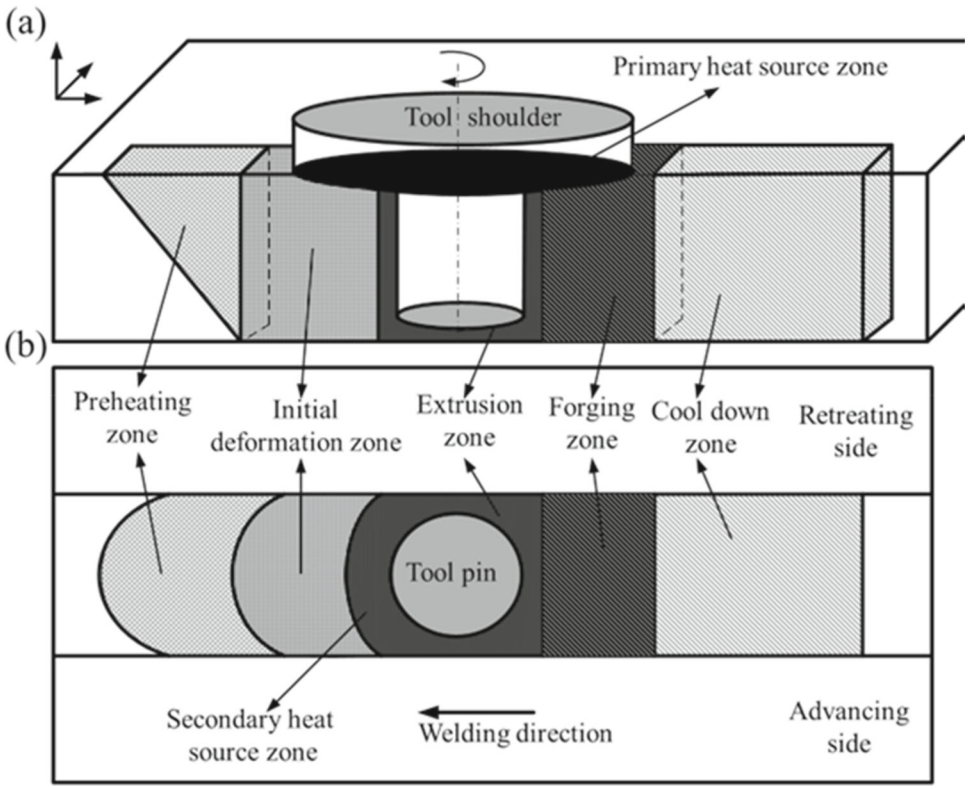

Fig. 2 Schematic representation of the mechanical deformation zone, primary and secondary heat impacted zones: Isometric view (**a**) and top view (**b**)

where μ is coefficient of friction and p is the plunging force applied by FSW tool.

The tool-workpiece interface's elemental area dA is used to represent the frictional heat generation [8]:

$$dQ_f = (1-\delta)\omega r \tau_{contact} dA \tag{5}$$

The amount of frictional effort dissipated into the workpiece is determined by r, which is the radial distance of elemental area dA from the axis. This distance accounts for the heat created by Q_p, plastic shear deformation adhering to the tool [2].

$$dQ_p = \delta \omega r \tau_{contact} dA \tag{6}$$

A mixed state is the last feasible state between the sticking and sliding conditions. When the matrix segment's velocity drops below the tool surface velocity, it stabilizes. Equilibrium is obtained when the internal yield shear stress equals the 'dynamic' contact shear stress because of a reasonably steady plastic deformation rate. The term "partial sliding/sticking situation" describes this. The friction coefficients for moving and static surfaces are equal under this concept. Therefore, the total heat produced as a result of sliding and sticking is shown as [19]:

$$Q_{FSW} = \delta * Q_{FSW,sticking} + (1-\delta) * Q_{FSW,sliding} \tag{7}$$

where δ is contact state variable, $Q_{FSW,sticking}$ is heat generation due to sticking condition and $Q_{FSW,sliding}$ is heat generation due to sliding condition.

Analytical expression on the welding tool's active surface is used to estimate how much heat is produced during FSW. An infinitesimal section on the shoulder surface is used to estimate the heat generation in that area as it rotates around the tool center axis. A uniform contact shear stress is applied to infinitesimal segment area dA = rdθdr. This section contributes with a torque of dM = rdF and an infinitesimal force of $dF = \tau_{contact} dA$. As seen in Fig. 3, the angle formed by this surface and the shoulder surface is the tool's active surface during the welding process. Q_1, Q_2, and Q_3 indicate the split of the heat energy created at the contact interface between a stationary workpiece and a revolving FSW tool, respectively. Since translational heat is significantly less strong than rotational heat, it can be disregarded in analysis. So, Q_{total} total heat generation is [18]

$$Q_{total} = Q_1 + Q_2 + Q_3 \tag{8}$$

where Q_1 is heat generation dur to shoulder with R_{probe} is inner radius and $R_{shoulder}$ is outer radius of tool shoulder and α is angle of inclination of shoulder surface [18].

$$Q_1 = \int_0^{2\pi} \int_{R_{probe}}^{R_{shoulder}} \omega \tau_{contact} r^2 (1 + tan\alpha) dr d\theta \tag{9}$$

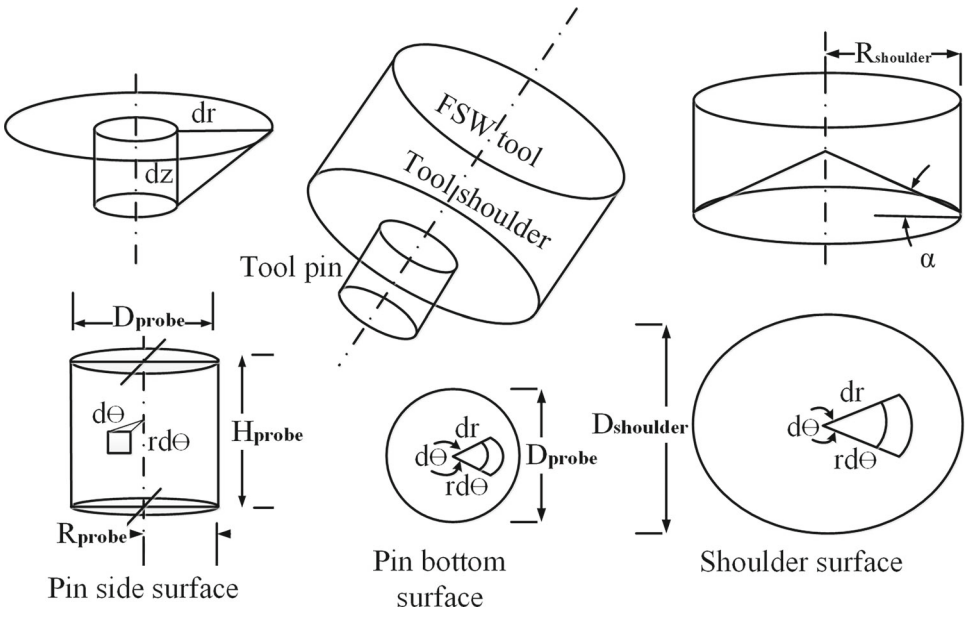

Fig. 3 Diagrammatic representation of the straight pin tool's nomenclature

where, the angle the conical shoulder creates is (Fig. 3). The probe's heat generation by probe vertical surface Q_2 is expressed as [18]:

$$Q_2 = \int_0^{2\pi} \int_0^{H_{probe}} \omega \tau_{contact} R_{probe}^2 dr d\theta = 2\pi\omega\tau_{contact} R_{probe}^2 H_{probe} \quad (10)$$

where H_{probe} is height of probe and R_{probe} is radius of probe. The probe's heat generation by probe bottom horizontal surface Q_2 is expressed as [18]:

$$Q_3 = \int_0^{2\pi} \int_0^{R_{probe}} \omega \tau_{contact} r^2 dr d\theta = \frac{2}{3}\pi\omega\tau_{contact} R_{probe}^3 \quad (11)$$

Consequently, the anticipated amount of heat produced overall by sliding or sticking friction is

$$Q = \frac{2}{3}\pi\omega\tau_{contact}\left(\left(R_{shoulder}^3 - R_{probe}^3\right) + R_{probe}^3 + 3R_{probe}^2 H_{probe}\right) \quad (12)$$

A linear combination of sliding and sticking circumstances results in the total heat generation for a flat shoulder and straight cylindrical tool, which is expressed as:

$$Q_{FSW} = \frac{2}{3}\pi\omega\left[\delta\tau_y + (1-\delta)\mu p\right]\left\{\left(R_{shoulder}^3 - R_{probe}^3\right) + R_{probe}^3 + 3R_{probe}^2 H_{probe}\right\} \quad (13)$$

where τ_y is yield shear stress and ω is angular velocity of tool.

Preheating source used in hybrid FSW are plasma arc and TIG arc. In plasma arc preheating, the workpiece surface is heated using a high-energy plasma arc. This preheating method helps the material plasticize, making it more receptive to the FSW tool's following mechanical action. Heat input (Q_p) is depended on current (I), voltage (V) and efficiency (μ_p) of plasma arc. Similar to this, TIG arc preheating incorporates a TIG welding arc's regulated heat input with efficiency (μ_{TIG}). The TIG arc delivers a targeted and accurate heat input to the area of interest in conjunction with an inert gas shield, preparing the material for the ensuing FSW process [18, 22].

The plasma arc's input for heat: $Q_p = \mu_p VI$

The TIG arc's input for heat : $Q_{TIG} = \mu_{TIG} VI$

A moving heat source capable of dispersing heat for FSW welding of materials that are similar and different. A circular surface heat source with an effective radius (r) serves as the model for the preheating source. The diameter of the plasma torch's nozzle and its distance from the plate surface determine the heat source's effective radius. However, the heat flux is given as and has a Gaussian distribution and expressed as

$$q_a(r) = \frac{3Q_{pre}}{\pi \underline{r}^2} e^{-3\left(\frac{r}{\underline{r}}\right)^2} \quad (14)$$

where Q_{pre} is total heat input (Q_p and Q_{TIG}) by preheating arc source. Typically, the thermal efficiency of plasma arc and TIG arc falls in the range of 70–90%. This means that a significant portion of the heat generated is effectively used for heat deposition on material, while a smaller proportion may be lost to factors like radiation, conduction, and convection. But, thermal efficiency of plasma is high due to a highly concentrated and hot plasma arc that can reach temperatures

Table 1 Heat calculation for FSW, TIG–FSW and Plasma-FSW according to the process parameters for aluminum alloy

Welding process	FSW	TIG–FSW	Plasma-FSW
Heat equation	$dQ_{FSW} = dQ_f$	$dQ_{P\text{-}FSW} = dQ_f + dQ_p$	$dQ_{TIG–FSW} = dQ_f + dQ_{TIG}$
Friction and plastic deformation heat input (J)	1750	1750	1750
Preheating input (J)	0	731.25	956.25
Total heat (J)	1750	2481.25	2706.25

much higher than those of a TIG arc. This high energy density allows for efficient heat input and effective melting of materials, contributing to a relatively high thermal efficiency (Table 1).

Understanding the ways by which heat is generated by different welding techniques is essential to the inquiry. The controlled rotation and translation of a specialized tool in FSW causes frictional heat to be produced. The integration of plasma arc and TIG arc preheating methods in Plasma-FSW and TIG–FSW, in contrast, adds a new level of complexity. With the help of these energy sources, workpieces can be specifically preheated before to the FSW process, changing temperature distributions, the plasticity of the material, and the way that the material flows. The complex interaction between these variables ultimately determines the features of the welded joints.

With the help of commercial software called ABAQUS, the heat transfer study for the FSW, TIG–FSW, and Plasma-FSW processes is performed. It is assumed that the model's solution domain is the rectangular plate. A brick element of type DCC3D8, with eight nodes, is used to mesh the workpiece domain element. For the FSW thermal model, the defined boundary condition is surface contact of the solution domain. At time zero, it is assumed that the workpiece has a constant temperature. The calculation's beginning condition is written as

$$T(x,\ y,\ z,\ 0) = T_i \tag{15}$$

where T_i is the atmospheric temperature at time $t = 0$.

Figure 4 depicts schematically the boundary interface of the workpiece domain. Except for the top surface with radiation, natural convective boundary conditions are taken into account at the workpiece's free surface. The thermal boundary condition is defined mathematically as:

Table 2 FSW, TIG–FSW and Plasma-FSW process parameters for welding

Welding process	FSW	Plasma-FSW	TIG–FSW
Welding velocity (mm/min)	63	63	63
Rotation of tool (RPM)	600	600	600
Preheating current (Amp)	0	45	45

FSW, TIG–FSW and Plasma-FSW:

$$k\frac{\partial T}{\partial n} = h(T - T_0) + \delta\theta\left(T_0^4 - T^4\right) - q_s - q_a \tag{16}$$

where k is the thermal conductivity of the workpiece, n is the normal direction vector of the boundary, h is the convection coefficient, q_s is the heat flow between the tool and the workpiece, and q_a is the heat flux from the plasma arc. The variables T_o, T, θ, and δ represent the ambient temperature, workpiece temperature, Stefan Boltzmann constant, and surface emissivity, respectively.

3 Experimental details

Experiments were conducted on vertical milling machine with fixture attached on the machine and plasma and TIG arc welding machine are used for preheating in Plasma-FSW and TIG–FSW hybrid FSW process as shown in Fig. 5. A workpiece made of aluminum 1100 with dimensions of 200 × 200 mm and a thickness of 6 mm was used for this study. The welding process involved the use of a specific tool with measurements of 18 mm for the shoulder, 6 mm for the pin, and 5.75 mm for the pin height. 600 RPM and 63 mm/min were used as the welding parameters. The welding operation was completed on a vertical milling machine, guaranteeing precision and control at all times. For preheating, other heat sources including a plasma arc at 45 amps and a TIG arc at 45 amps were also used. This extensive setup enabled a thorough examination of the thermal behavior and efficiency of the FSW process, particularly two thermocouples were attached on the workpiece in advancing side and retreading side at 5 mm from tool shoulder edge. Table 2 lists three experimental conditions.

4 Result and discussion

The experimental thermal histories of all three Friction Stir Welding (FSW) variants are shown in a single figure as shown in the Fig. 6. The graph depicts the temperature profiles over

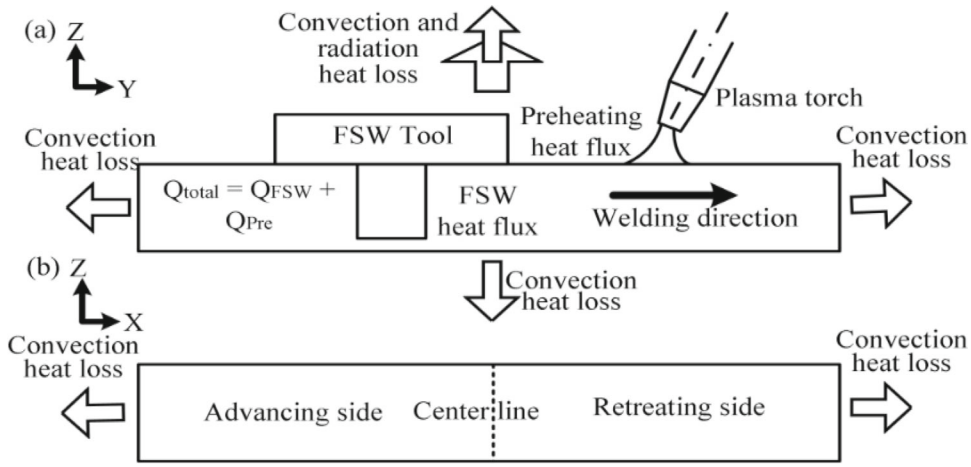

Fig. 4 Representation of heat transfer model thermal boundary condition

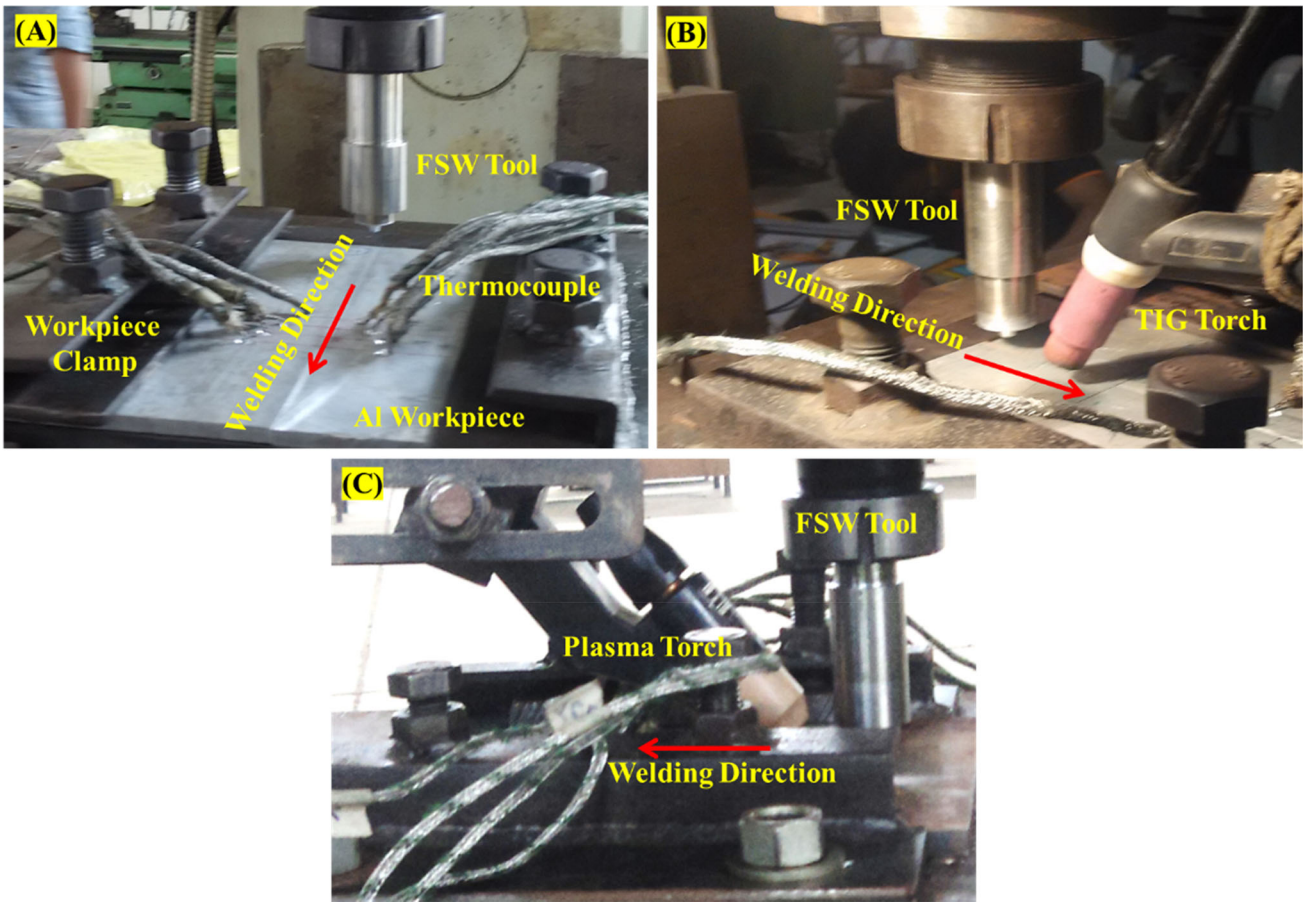

Fig. 5 Experimental setup for **a** FSW, **b** TIG–FSW, and **c** Plasma-FSW

time for FSW, Plasma-FSW, and TIG–FSW during the welding process. A separate curve or line on the graph represents the temperature history of each welding variant. Figure 5b, c demonstrate how, the welding process advances from 0 to 200 s, the temperature profile slop increases at preheating zone locations inside the weld zone as compare to FSW due to preheating by plasma and TIG. The graphic illustrates the differences between the three welding methods' thermal behavior with respect to time and temperature profile not change much but in preheating condition slop is stiffer in cooling zone due to high cooling rate. Additional heat input due to preheating improve the plasticization temperature by 6% ahead of FSW tool. Peak temperature achieved at TC1 is 314.1 °C, 333.1 °C and 345.2 °C respectively in FSW,

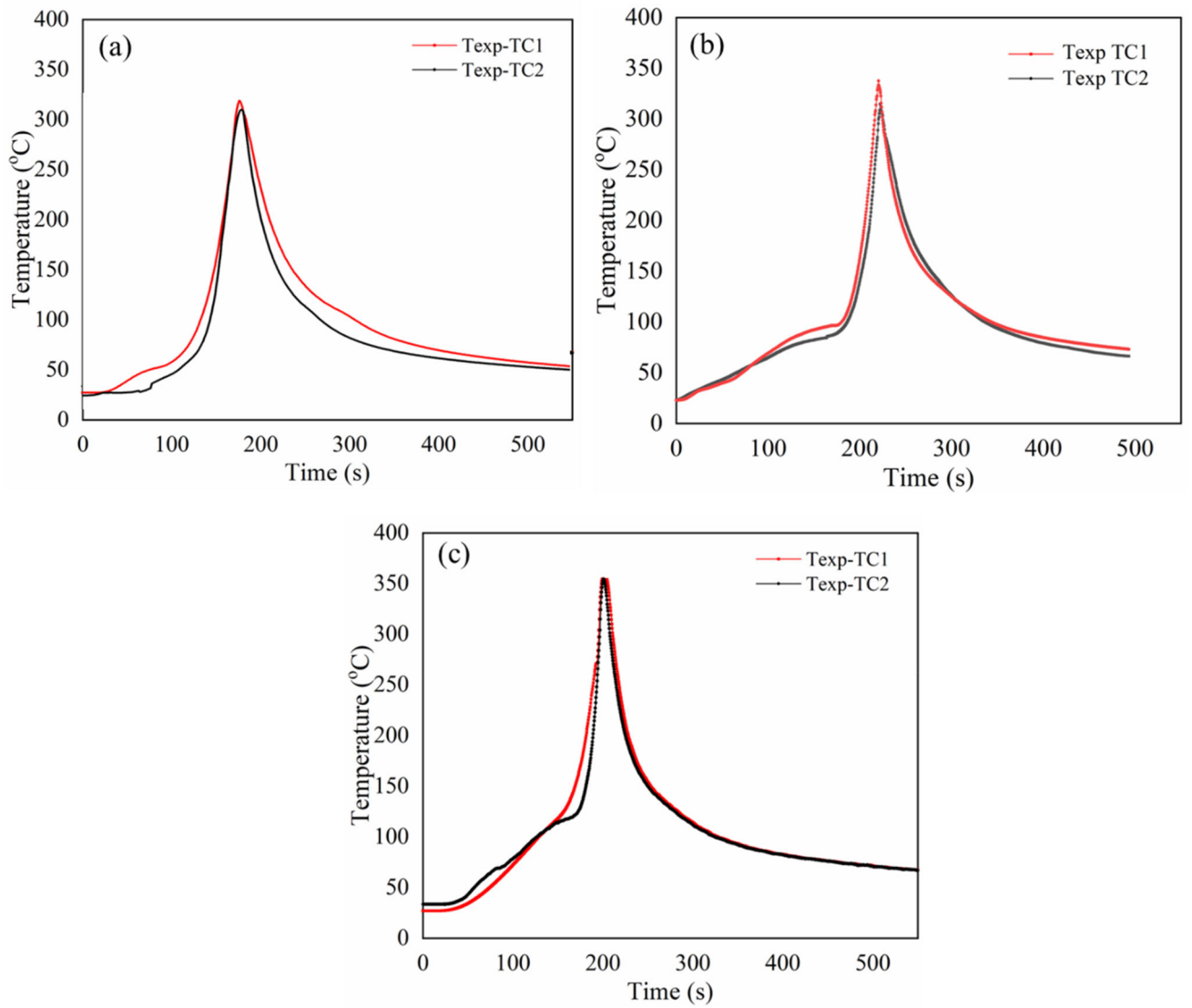

Fig. 6 Comparative thermal history of all three variant **a** FSW **b** TIG–FSW **c** Plasma-FSW

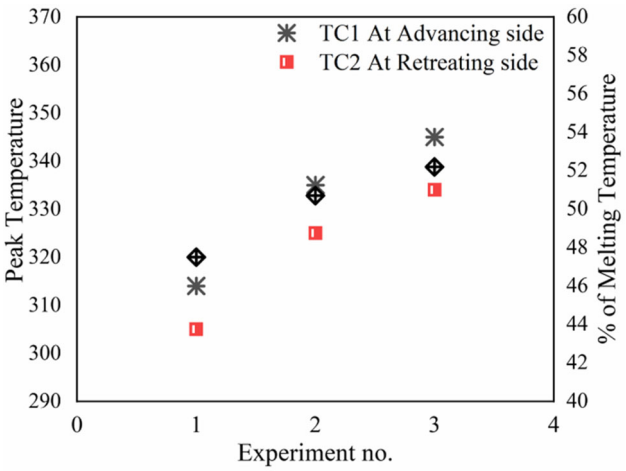

Fig. 7 Illustration of peak temperature and percentage of melting point achieved during three variants of welding

TIG–FSW and Plasma-FSW which shows improvement in thermal state of welding material. In order to fully grasp the comparison between heat input and thermal history of FSW and hybrid FSW provide relative information about grain size and mechanical properties achieved during three different welding condition. Preheating provides additional heat which help to welding material without defect at low rotational speed and high welding speed. For the reason that preheating improves the total heat input during welding and enhance the material flow around the FSW tool.

The relevant Fig. 7 displays comparative data of peak temperature as a percentage of the melting point of the workpiece material and shows highest temperatures reached during the welding process for each of the three FSW versions. On the graph, FSW peak temperature is each welding variation is represented by a unique data point. In plain FSW the peak

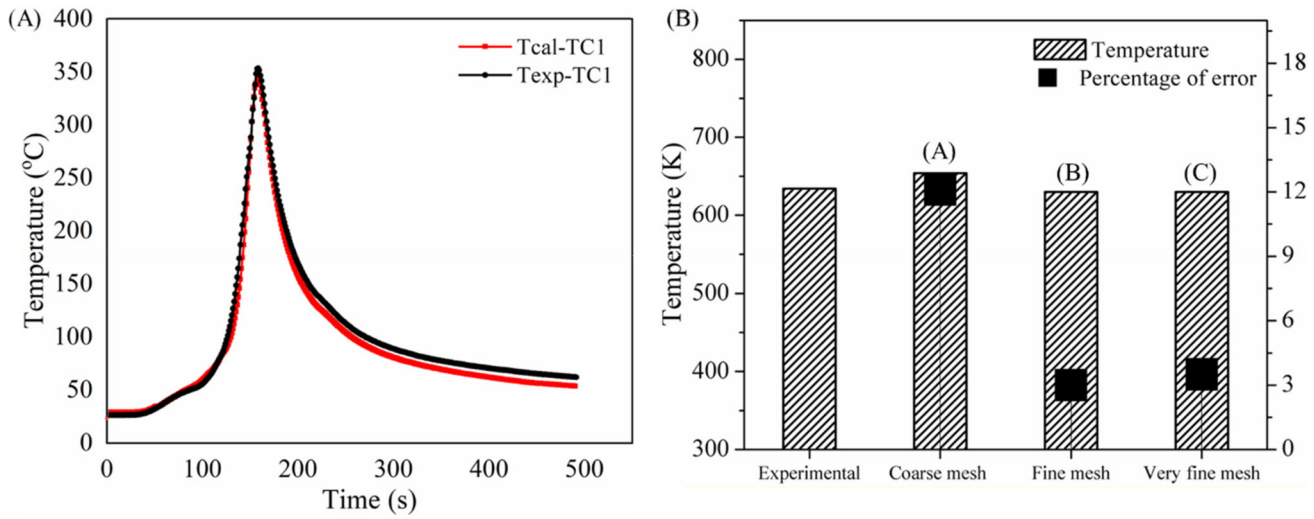

Fig. 8 **A** Comparison between experimental and calculated time temperature profile on the advancing side of FSW TC1. **B** The highest temperature measurements made at TC1 with various meshes were compared to the experimental values in the weld zone

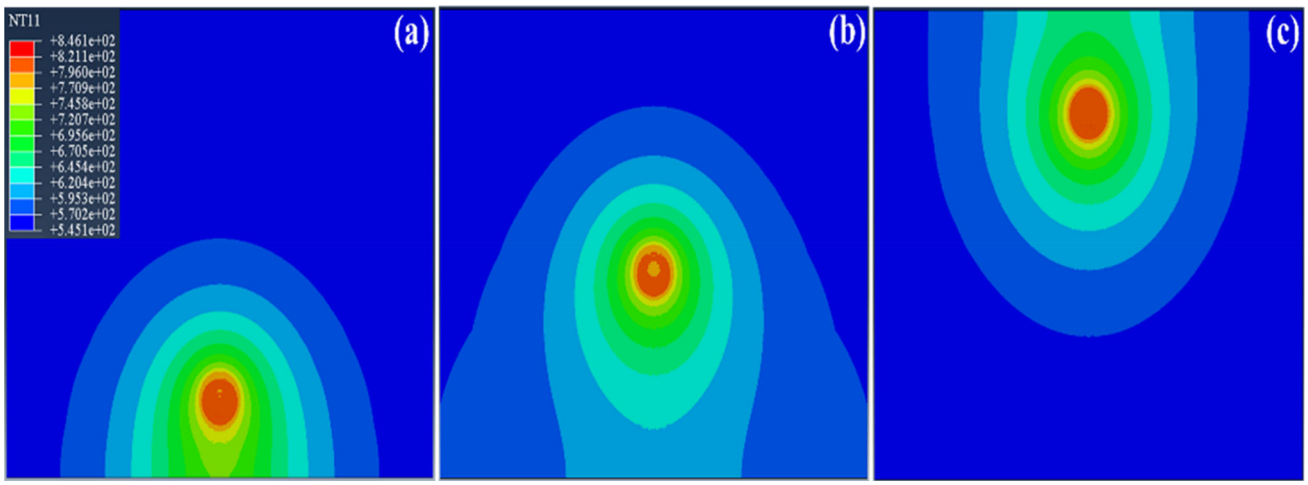

Fig. 9 3D isometric simulation results of FSW

temperature observed by thermocouple is 314.5 °C in advancing side and 307.1 °C in retreating side. While in TIG–FSW and Plasma-FSW achieve higher temperature due to preheating. In TIG–FSW peak temperature attended is 333.4 °C and Plasma-FSW achieved 345.7 °C in advancing side. Plasma-FSW attain higher temperature as compare to other variant with same FSW parameters due to high arc efficiency of plasma arc. The percentages are also computed in relation to the fusion point of the base material, giving a comparison of how close each welding method is to plasticization stage of the base material. The percentage of melting point with respect to peak temperature is 44.4% in case of FSW, which is lowest and ideate inadequate plasticization of weld material. Whereas in case of hybrid FSW the plasticization stage is improved up to 50 to 55% due to additional heat added by preheating source.

The thermal parameters of FSW, Plasma-FSW, and TIG–FSW are clearly illustrated in this image, allowing for a direct comparison of their heat generation. It offers important insights into the temperature management and effectiveness of these welding techniques in respect to the characteristics of the base metal [14–16].

The experiment is replicated in the physical modelling process, and the temperature profiles in the defined regions are obtained from the numerical solution. Therefore, analytical modelling is breaks down the FSW process into five temporal phases: plunge, initial dwell, welding, final dwell, and plunge-out. A 15 s dwell time is allotted in this simulation to heat the sample and facilitate the welding process. A 5 s dwell time is then set aside to facilitate the tool's easy withdrawal from the workpiece. On the bases of this time step, determine peak welding temperatures and temperature profiles during thermal analysis, a numerical simulation is

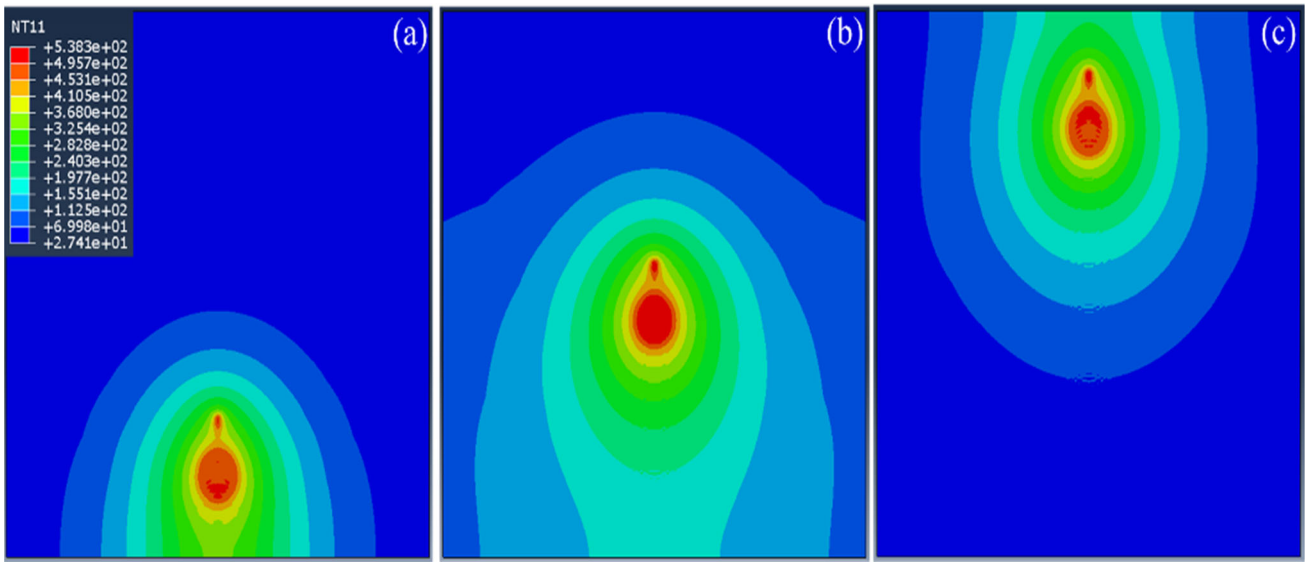

Fig. 10 3D isometric simulation results of TIG–FSW

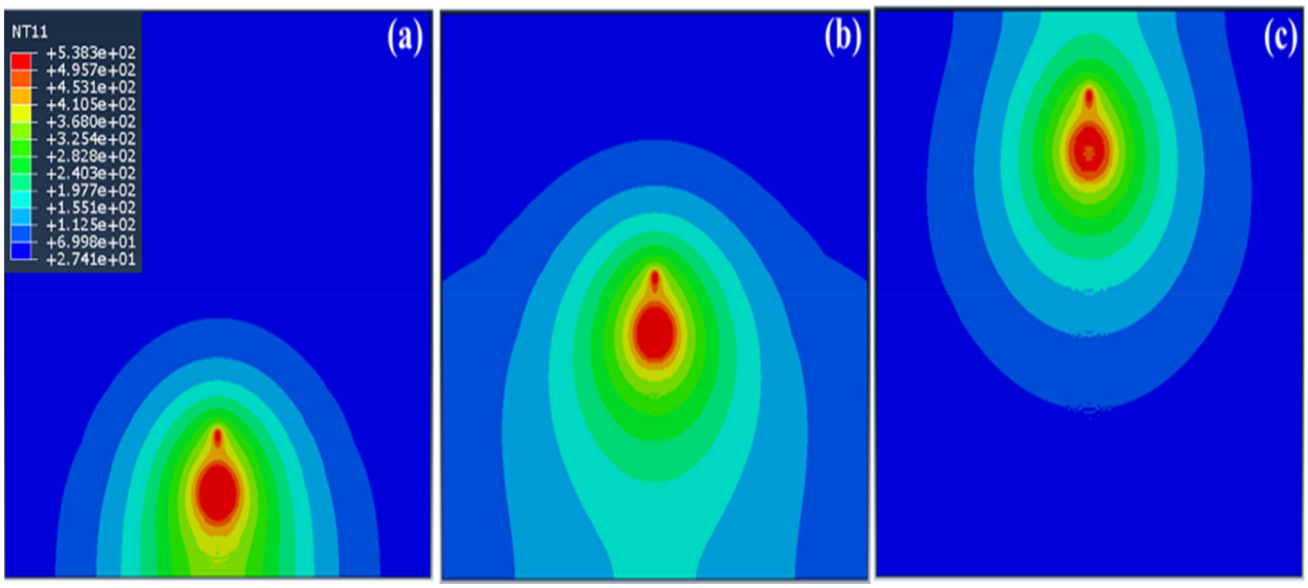

Fig. 11 3D isometric simulation results of Plasma-FSW

used to examine the behavior of an aluminum alloy under three different welding settings as mention in Table 1. The time–temperature histories of FSW TC1 thermocouple point chosen for analysis are shown in Fig. 8A. In order to choose an appropriate element size that would accurately model the FSW process at the lowest possible computing cost, a mesh sensitivity analysis was also carried out. As seen in Fig. 8B, three mesh sizes were taken into consideration in the weld zone: coarse mesh (0.0001 m), fine mesh (0.0005 m), and very fine mesh (0.00025 m). As shown in Fig. 8B, the peak temperatures measured at the position of TC1 using these three meshes were compared to the experimental values together with the percentage of error. It was discovered that FE modelling with Mesh A overestimates the experimental peak temperature at the thermocouple position by more than 1.2 percent. However, the peak temperatures that Mesh B and Mesh C anticipated were similar.

The three-dimensional isometric perspective of the simulation findings for FSW, TIG–FSW, and Plasma-FSW were shown in FigS. 9, 10, and 11, respectively. The complex intricacies of the simulated weld zones for all their variant at welding time 40 s(a), 150 sce(b) and 240 s(c) are probably on display. The simulation outcome for each welding alternative is shown in a different time of welding, enabling easy comparison. The three-dimensional perspective offers perceptions into the temperature profile, temperature distribution, and temperature contours. During hybrid FSW a

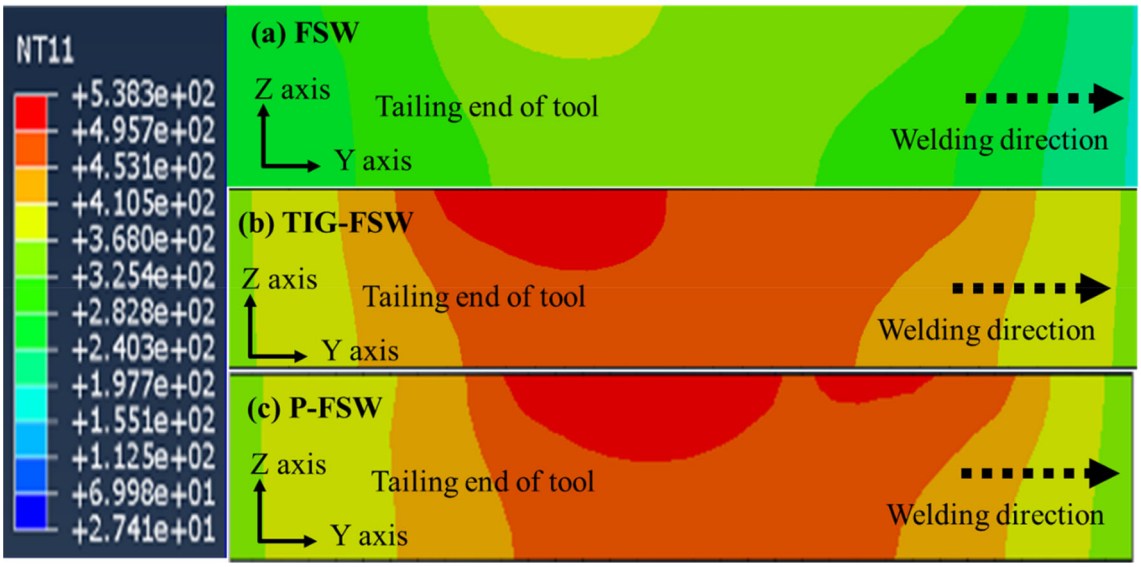

Fig. 12 Cross sectional view of simulated results for **a** FSW **b** TIG–FSW and **c** Plasma-FSW

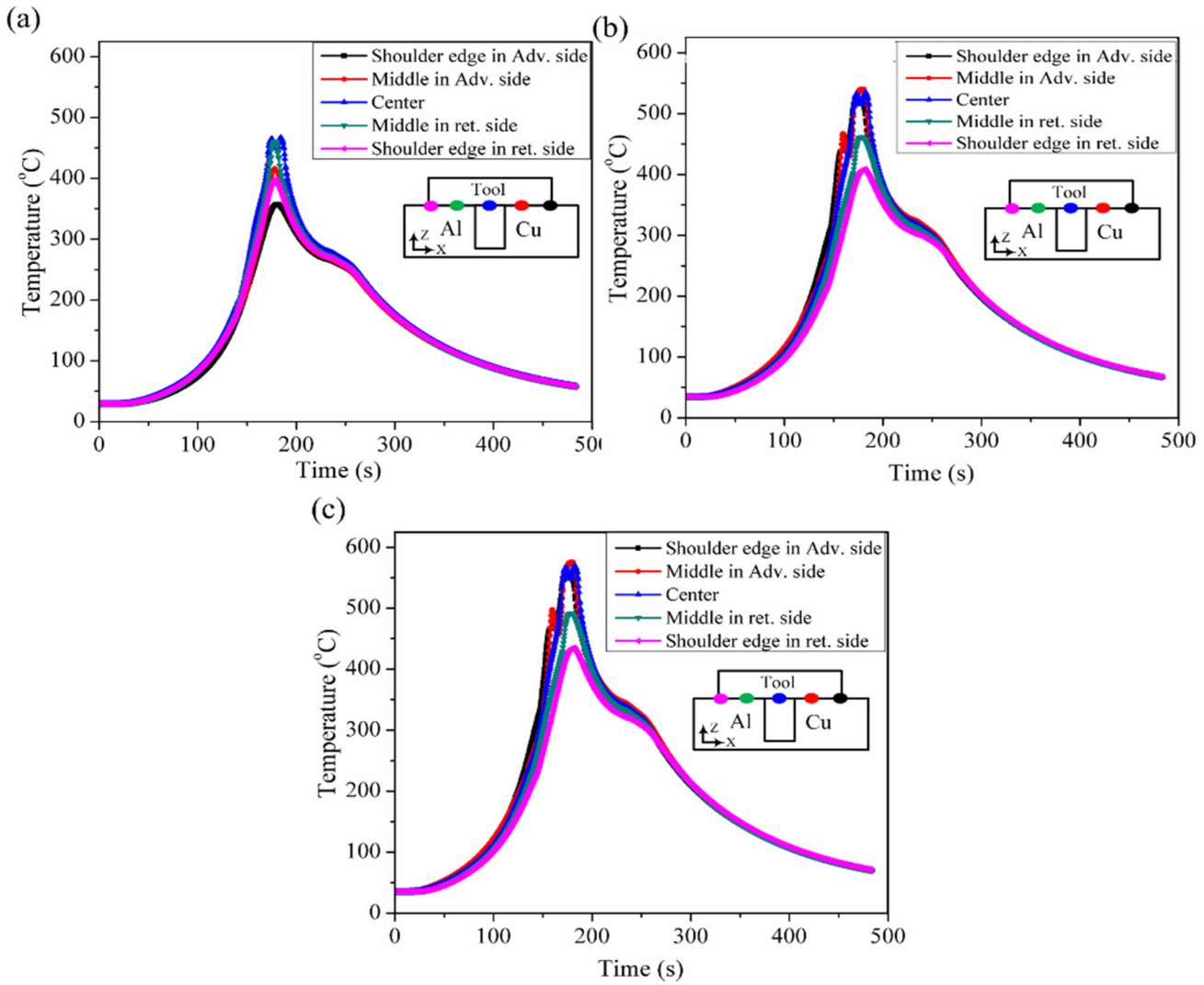

Fig. 13 Calculated thermal history under the shoulder for **a** FSW **b** TIG–FSW and **c** Plasma-FSW

preheating source is moving ahead of FSW heat source which improve thermal state of material ahead of FSW tool. These preheating indirectly improve efficiency of welding process in respect of less defect and high joint strength.

The temperature distribution for all three variants is shown in Fig. 12 in transverse directions. Due to differences in heat generation as well as tool and material movement, the temperature distribution in the stirring zone is not symmetrical. Preheating or using an external heating source increases material flow and lengthens the process window for a good weld connection in the hybrid FSW process [11–16]. Figure 12b, c depicts the contrast among the experimental and simulated weld zones of TIG–FSW and Plasma-FSW. The calculated isotherm shows in case of Plasma-FSW archives high temperature as compare to TIG–FSW. In FSW, stir of material in the weld zone is difficult as the inadequate temperature that is reached in case of FSW and in little extent TIG–FSW is insufficient to plasticize the material. As a result, there is a very high likelihood that the contact may develop a fault and voids. Without preheating, there are many voids and flaws created in the nugget zone during low parameters of FSW. It is clear that the temperature isotherm offers helpful knowledge regarding different weld precincts. The auxiliary heat source assisted in improvement in material flow and heat generation.

The predicted temperature history beneath the shoulder at various points within the solution geometry is shown in Fig. 13. Figure 13a shows a time–temperature profile without preheating, while Fig. 13b, c shows the same profile with preheating from a plasma arc and TIG arc. The 45 Amp plasma arc and TIG arc of the preheating source raise the temperature of the material ahead of the FSW tool by an additional 45 to 70 °C at time period 175 s in the time–temperature curve. The temperature rise beneath the tool's shoulder plasticizes the material and refines the grains through a process known as recrystallization. As a result, research is done to determine the flow stress value and temperature distribution at the contact [5, 19–23].

This research work enables a thorough understanding of the design aspect, thermal behaviors and temperature distributions of FSW, Plasma-FSW, and TIG–FSW through comparison of their respective thermal histories. It helps researchers and engineers better understand how different welding processes effect temperature changes in the weld zone by giving them insightful information [16–18]. There are notable differences in heat input, thermal behavior, and weld properties between FSW, Plasma-FSW, and TIG–FSW when welding aluminium. Higher peak temperatures and distinct thermal gradients have been created within the weldment as a result of the incorporation of auxiliary heat sources, particularly the powerful plasma arc in Plasma-FSW.

5 Conclusions

The comparative thermal analysis presented in this research work to provide empathizes on the thermal behavior and temperature distributions of three friction stir welding (FSW) variants: FSW, Plasma-FSW, and TIG–FSW. Through comprehensive examination of their thermal histories, peak temperatures, and simulated weld zones, the research elucidates the impact of auxiliary heat sources on heat input and material flow.

- The results of the analysis showed that the employment of auxiliary heat sources has a significant improvement in the thermal behavior and appropriate temperature and temperature profiles achieved.
- Temperature achieved at thermocouple during experiment are 314.5 °C and 307.1 °C (TC1 advancing side and TC2 retreating side respectively) in FSW while, during TIG–FSW and Plasma-FSW achieved temperatures of 333.4 °C and 345.7 °C, respectively in the advancing side.
- FSW achieved 44.4% of melting temperature of base metal at TC1, indicating insufficient plasticization, whereas hybrid FSW variants achieved percentages between 50 and 55%, indicating enhanced plasticization as a result of the additional heat provided by preheating sources.
- Plasma-FSW achieved higher peak temperatures than other approaches during analytical results due to the focused and high-energy nature of the plasma arc preheating and creating a preheated zone with higher temperatures.
- The auxiliary source preheating was crucial for adjusting the plasticized material's characteristics and regulating the heat input before the FSW process.
- Particularly in the context of aluminium welding, the complex interactions between heat input variations and the welding process have been clarified. As a result, it has become evident how differences in heat input affect thermal behavior and weld properties.

These findings expand the further research in hybrid FSW ought to delve into a variety of materials and geometries, incorporate third materials for combined improvement, and investigate advance machine learning models for accurate prediction and parameters optimizations. These initiatives will promote efficiency and innovation in welding technology for a range of industrial applications by enhancing predictive capacities and streamlining welding procedures.

Funding This research is not funded by any sponsored agency.

Data availability All data and materials used to produce the results in this article can be obtained upon request from the corresponding authors.

Declarations

Conflict of interests The authors declare that they have no conflict of interest to report.

Consent for publication The authors declare that all authors agree to sign the transfer of copyright for the publisher to publish this article upon acceptance.

References

1. Padhy, G.K., Wu, C.S., Gao, S.: Auxiliary energy assisted friction stir welding – Status review. Sci. Technol. Weld. Join. **20**(8), 631–649 (2015)
2. Yaduwanshi, D.K., Bag, S., Pal, S.: Numerical modeling and experimental investigation on plasma-assisted hybrid friction stir welding of dissimilar materials. Mater. Des. **92**(92C), 166–183 (2016)
3. Liu, X.C., Wu, C.S.: Material flow in ultrasonic vibration enhanced friction stir welding. J. Mater. Process. Technol. **225**, 32–44 (2015)
4. Msomi, V., Mabuwa, S.: Analysis of material positioning towards microstructure of the friction stir processed AA1050/AA6082 dissimilar joint. Adv. Ind. Manuf. Eng. **1**, 100002 (2020)
5. Mehdi, H., Mishra, R.S.: Influence of friction stir processing on weld temperature distribution and mechanical properties of TIG-welded joint of AA6061 and AA7075. Trans. Indian Inst. Met. **73**, 1773–1788 (2020)
6. Msomi, V., Mbana, N.: Mechanical properties of friction stir welded AA1050-H14 and AA5083-H111 joint: sampling aspect. Metals **10**(2), 214 (2020)
7. Spinella, D.J., Streicher, E.T., & Kastelic, R.: Resistance Heated Stir Welding, US Patent No. 5 829664, published 3 November 1998.
8. Ferrando, W.A.: Electrically Assisted Friction Stir Welding, The United States of America as Represented by the Secretary of the Navy, Washington, DC, USA, US Patent No. 8 164 021 B1, published 21 April 2012.
9. Long, X., Khanna, S.K.: Modelling of electrically enhanced friction stir welding process using finite element method. Sci. Technol. Weld. Join. **10**, 482–487 (2005)
10. Luo, J., Li, F., Chen, W.: Experimental researches on resistance heat aided friction stir welding of Mg alloy. Q. J. Jpn. Weld. Soc. **31**, 65–68 (2013)
11. Santos, T.G., Miranda, R.M., Vilaca, P.: Friction stir welding assisted by electrical joule effect to overcome lack of penetration in aluminium alloys. Key Eng. Mater. **611**, 763–772 (2014)
12. Santos, T.G., Miranda, R.M., Vilaca, P.: Friction stir welding assisted by electrical Joule effect. J. Mater. Process. Technol. **214**, 2127–2133 (2014)
13. Potluri, H., Jones, J.J., & Mears, L.: Comparison of Electrically Assisted and Conventional Friction Stir Welding Processes by Feed Force and Torque'. Proc. ASME 2013 Int. Manufacturing Science and Engineering Conf., Madison, WI, USA, June 2013, ASME, Paper MSEC2013–1192.
14. Liu, X., Lan, S., Ni, J.: Electrically assisted friction stir welding for joining Al 6061 to TRIP780 steel. J. Mater. Process. Technol. **219**, 112–123 (2015)
15. Tang, W., Guo, X., McClure, J.C., Murr, L.E., Nunes, A.: Heat input and temperature distribution in friction stir welding. J. Mater. Process. Manuf. Sci. **7**(2), 163–172 (1988)
16. Yaduwanshi, D.K., Bag, S., Pal, S.: Heat transfer analyses in friction stir welding of aluminum alloy. Proc. IMechE Part B J. Eng. Manuf. **23**, 3794–3803 (2014)
17. Yaduwanshi, D.K., Bag, S., Pal, S.: On the effect of tool offset in hybrid FSW of copper and aluminium alloy. Mater. Manuf. Process. **33**(3), 277–287 (2018)
18. Yaduwanshi, D.K., Bag, S., Pal, S.: Numerical modeling and experimental investigation on plasma- assisted hybrid friction stir welding of dissimilar materials. Mater. Design **92**, 166–183 (2016)
19. Nandan, R., Roy, G., Lienert, T., DebRoy, T.: Numerical modelling of 3D plastic flow and heat transfer during friction stir welding of stainless steel. Sci. Technol. Weld. Join. **11**, 526–537 (2006)
20. Zhang, Z., Chen, J.T., Zhang, Z.W., Zhang, H.W.: Coupled thermo-mechanical model-based comparison of friction stir welding processes of AA2024-T3 in different thicknesses. J. Mater. Sci. **46**, 5815–5821 (2011)
21. Fonda, R.W., Lambrakos, S.G.: Analysis of friction stir welds using an inverse problem approach. Sci. Technol. Weld. Join. **7**(3), 177–181 (2002)
22. Mehdi, H., Batra, L., Singh, A.P., Malla, C.: Multi-response optimization of FSW process parameters of dissimilar aluminum alloys of AA2014 and AA6061 by response surface methodology (RSM). Int. J. Interact. Design Manuf. (IJIDeM). **27**, 1–6 (2023)
23. Mabuwa, S., Msomi, V.: Effect of friction stir processing on gas tungsten arc-welded and friction stir-welded 5083–H111 aluminium alloy joints. Adv. Mater. Sci. Eng. **2019**, 1–4 (2019)
24. Yaduwanshi, D.K., Bag, S., Pal, S.: Effect of preheating in hybrid friction stir welding of aluminum alloy. J. Mater. Eng. Perform. **23**, 1–12 (2014)
25. Boukraa, M., Chekifi, T., Lebaal, N., Aissani, M.: Robust optimization of both dissolution time and heat affected zone over the friction stir welding process using SQP technique. Exp. Tech. **46**, 677–689 (2021)
26. Boukraa, M., Lebaal, N., Mataoui, A., Settar, A., Aissani, M., Tala-Ighil, N.: Friction stir welding process improvement through coupling an optimization procedure and three-dimensional transient heat transfer numerical analysis. J. Manuf. Process. **34**(A), 566–578 (2018)
27. Boukraa, M., Chekifi, T., Lebaal, N.: Friction stir welding of aluminum using a multi-objective optimization approach based on both Taguchi method and grey relational analysis. Exp. Techn. **47**(3), 603 (2023)
28. Boukraa, M., Bassir, D., Lebaal, N., Chekifi, T., Aissani, M., Ighil, T., Mataoui, A.: Thermal analysis of the friction stir welding process based on boundary conditions and operating parameters. Proc. Est. Acad. Sci. **70**(4), 516 (2021)
29. Madani, A., Boukraa, M., Aissani, M., Chekifi, T., Ziadi, A., Zirari, M.: Experimental investigation and numerical analysis using Taguchi and ANOVA methods for underwater friction stir welding of aluminium alloy 2017 process improvement. Int. J. Press. Vessels Pip. **201**, 104879 (2023)
30. Boukraa, M., Aissani, M., Lebaal, N., Bassir, D., Mataoui, A., Tal-Ighil, N., Yue, H.: Effects of boundary conditions and operating parameters on temperature distribution during the friction stir welding process. IOP Conf. Ser. Mater. Sci. Eng. **1140**, 012050 (2021)